

Response assessment during chemoradiation using a hypercellular/hyperperfused imaging phenotype predicts survival in patients with newly diagnosed glioblastoma

Michelle M. Kim, Madhava P. Aryal, Yilun Sun, Hemant A. Parmar, Pin Li, Matthew Schipper, Daniel R. Wahl, Theodore S. Lawrence, and Yue Cao

Department of Radiation Oncology, The University of Michigan, Ann Arbor, Michigan, USA (M.M.K., M.P.A., Y.S., M.S., D.R.W., T.S.L., Y.C.); Department of Biostatistics, The University of Michigan, Ann Arbor, Michigan, USA (Y.S., P.L., M.S.); Department of Radiology, The University of Michigan, Ann Arbor, Michigan, USA (H.A.P., Y.C.); Department of Biomedical Engineering, The University of Michigan, Ann Arbor, Michigan, USA (Y.C.)

Corresponding Authors: Michelle M. Kim, MD, Department of Radiation Oncology, University of Michigan, 1500 E. Medical Center Dr., Ann Arbor, MI 48109-0010, USA (michekim@med.umich.edu); Statistical support: Yilun Sun, PhD, Department of Biostatistics, The University of Michigan, 4417B Med Sci I, 1301 Catherine St, Ann Arbor, MI 48109, USA (yilunsun@med.umich.edu).

Abstract

Background. Adversely prognostic hypercellular and hyperperfused regions of glioblastoma (GBM) predict progression-free survival, and are a novel target for dose-intensified chemoradiation (chemoRT) recently implemented in a phase II clinical trial. As a secondary aim, we hypothesized that dose-intensified chemoRT would induce greater mid-treatment response of hypercellular/hyperperfused tumor regions vs standard chemoradiation, and that early response would improve overall survival (OS).

Methods. Forty-nine patients with newly diagnosed GBM underwent prospective, multiparametric high b value diffusion-weighted MRI (DW-MRI) and perfusion dynamic contrast-enhanced MRI (DCE-MRI) pre-RT and 3-4 weeks into RT. The hypercellular tumor volume (TV_{HCV} , mean contralateral normal brain + 2SD) and hyperperfused tumor volume (TV_{CBV} , contralateral normal frontal gray matter + 1SD) were generated using automated thresholding. Twenty-six patients were enrolled on a dose-escalation trial targeting TV_{HCV}/TV_{CBV} with 75 Gy in 30 fractions, and 23 non-trial patients comprised the control group. OS was estimated using the Kaplan-Meier method and compared using the log-rank test. The effect of TV_{HCV}/TV_{CBV} and Gd-enhanced tumor volume on OS was assessed using multivariable Cox proportional-hazard regression.

Results. Most patients had gross total (47%) or subtotal resection (37%), 25% were MGMT-methylated. Patients treated on the dose-escalation trial had significantly greater reduction in TV_{HCV}/TV_{CBV} (41% reduction, IQR 17%-75%) vs non-trial patients (6% reduction, IQR 6%-22%, $P = .002$). An increase in TV_{HCV}/TV_{CBV} during chemoRT was associated with worse OS (adjusted hazard ratio [aHR] 1.2, 95%CI 1.0-1.4, $P = .02$), while pre-treatment tumor volumes ($P > .5$) and changes in Gd-enhanced volume ($P = .9$) were not.

Conclusions. Multiparametric MRI permits identification of therapeutic resistance during chemoRT and supports adaptive strategies in future trials.

Key Points

1. A novel MR biomarker identifies hypercellular, hyperperfused glioblastoma regions.
2. Mid-treatment biomarker response to dose-escalated radiation yields superior survival.
3. Early response assessment and adaptive radiation may target treatment resistance.

Importance of the Study

Adversely prognostic hypercellular and hyperperfused tumor regions in glioblastoma identified using high b value diffusion-weighted MRI and dynamic contrast-enhanced perfusion MRI have been implemented as a novel target for radiation dose-intensification in a recent phase II clinical trial. In this study, we demonstrate the dose-response of this imaging signature during the course of radiation therapy, and the association of the mid-treatment hypercellular/hyperperfused tumor

volume with survival and tumor recurrence. These findings suggest that a multiparametric MR imaging technique to identify hypercellular and hyperperfused tumor regions during the course of radiation may potentially be used for early response assessment and adaptive treatment strategies that selectively target persistent and developing regions of treatment resistance in future studies.

With few advancements in the treatment of glioblastoma (GBM) over the last 2 decades, a persistent limitation remains the lack of biologically informed imaging that can specifically detect response or progression *during* standard therapies. The perennial difficulty of assessing tumor status after chemoradiation (chemoRT) using conventional T1-weighted gadolinium-enhanced (T1-Gd) and fluid-attenuated inversion recovery (FLAIR) MRI has prompted numerous studies incorporating advanced metabolic and physiologic imaging techniques to more reliably assess tumor status after completion of radiation therapy.^{1,2} However, few efforts have been devoted to discovering whether tumor changes during the course of chemoradiation can be detected using conventional or advanced imaging techniques, and whether such changes are correlated with patient outcome. Such a non-invasive biomarker would permit early potential adaptation or intensification of radiation or combined therapies to help overcome treatment resistance.

In an effort to develop and implement an imaging technique with potential to elucidate persistent and developing regions of treatment resistance before and during radiation and to feasibly perform as a routine imaging protocol, we reported on a multiparametric MR imaging signature incorporating high b value diffusion-weighted (DW) MRI and dynamic contrast-enhanced (DCE) MRI for patients with newly diagnosed GBM.^{3,4} Using this advanced MRI technique to detect hypercellular (TV_{HCV}) and hyperperfused (TV_{CBV}) tumor regions (Figure 1) after surgical resection, we demonstrated that this combined imaging phenotype identified tumor regions highly likely to progress after standard chemoradiation, its association with progression-free survival (PFS), and its spatial correlation with eventual tumor recurrence (Supplementary Figure 1).^{3,4} Moreover, because 40% of the tumor identified with this technique was non-enhancing, the hypercellular/hyperperfused tumor regions were often excluded from the radiation boost volume defined using conventional MRI. In a phase II clinical trial (NCT02805179) reported separately,⁵ we investigated whether targeting the residual, postoperative hypercellular/hyperperfused TV_{HCV}/TV_{CBV} identified prior to radiation with dose-intensified chemoRT to 75 Gy improved outcomes in patients with GBM (Supplementary Figure 2).

As a secondary aim reported herein, we assessed the responsiveness of hypercellular/hyperperfused GBM tumor regions during the radiation treatment course and its correlation with survival. We hypothesized that in contrast

to standard chemoradiation, dose-intensified chemoRT would induce greater reduction or response of adversely prognostic hypercellular/hyperperfused tumor regions, and that early response would translate into improved overall survival (OS). These findings would then inform future trials incorporating this imaging signature for adaptive treatment modification during the course of radiation therapy to overcome treatment resistance and improve outcomes in GBM.

Methods

Patient Cohorts

Forty-nine patients with pathologically confirmed, newly diagnosed GBM underwent multiparametric MRI scans on prospective, IRB-approved protocols (NCT02805179 and NCT01988675) following maximal surgical resection. All patients underwent multiparametric MRI prior to chemoradiation, and again during the 3rd-4th weeks of chemoradiation. Twenty-six patients were enrolled on a dose-escalation phase II trial (NCT02805179) targeting the hypercellular/hyperperfused tumor regions identified by multiparametric MRI. The remaining 23 patients comprised a similar population to the dose-escalation trial cohort, and were enrolled on a corollary imaging study (NCT01988675) and treated per institutional standard of care based on conventional MRI (T1-weighted gadolinium-enhanced and T2-FLAIR), without specific regard to advanced MR imaging (hereafter referred to as the non-trial cohort).

Chemoradiation Treatment

All patients were treated using intensity-modulated or volumetric-modulated arc therapy to the surgical cavity and residual T1-weighted gadolinium-enhanced abnormality (TV_{Gd}), which was expanded by approximately 1.7 cm to create a clinical target volume (CTV) and 0.3 cm for planning target volume (PTV) (a total of 2-cm margin, analogous to the approach used by the European Organisation for Research and Treatment of Cancer [EORTC]).⁶ The PTV was most commonly prescribed 60 Gy in 30 fractions, and T2-FLAIR was not specifically targeted to 60 Gy unless bulky non-enhancing disease was identified (<5% of cases). Patients treated on the phase II dose-escalation trial were likewise treated to 60

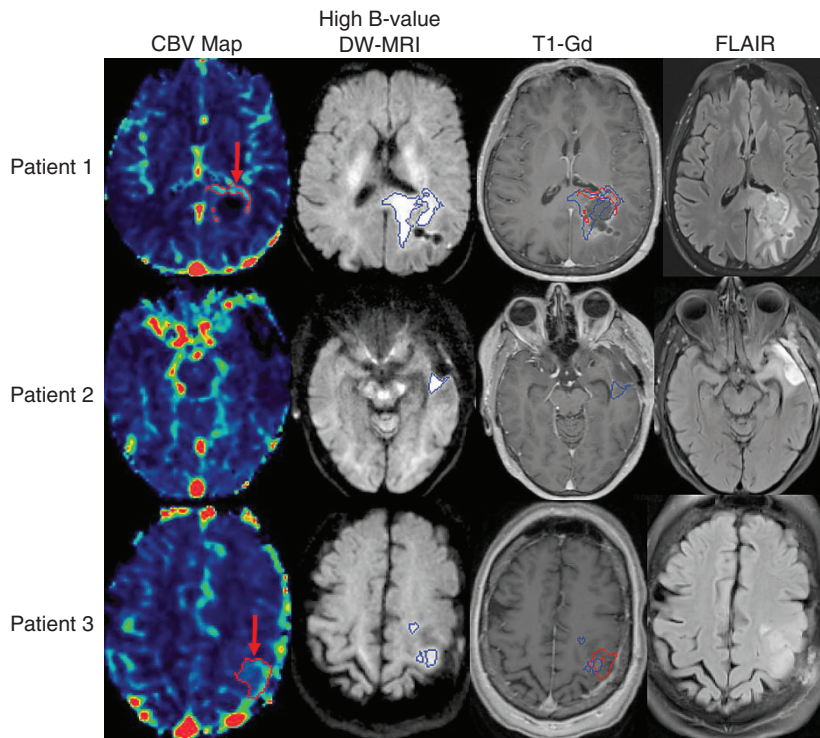


Fig. 1 In the top row, representative images from Patient 1 demonstrate hyperperfused tumor (red arrow, first column) identified with dynamic contrast-enhanced MRI, and hypercellular tumor (blue volume, second column) identified with high b value diffusion-weighted MRI. Both volumes are overlaid on the T1-weighted gadolinium-enhanced MRI (third column), and the non-enhancing hypercellular tumor extends across the splenium. In the middle row, the left temporal lobe tumor from Patient 2 demonstrates residual, non-enhancing hypercellular tumor posterior to the surgical cavity (blue volume, second column) without corresponding hyperperfusion. This non-enhancing tumor region is significantly smaller than the nonspecific FLAIR hyperintensity surrounding the cavity (last column). In the bottom row, representative images from Patient 3 demonstrate both hyperperfused (red arrow, first column) and hypercellular (blue volume, second column) tumor in the left posterior frontal lobe that was non-enhancing and superior to the surgical cavity. Abbreviations: CBV, cerebral blood volume; DW-MRI, diffusion-weighted magnetic resonance image; FLAIR, fluid-attenuated inversion recovery; T1-Gd, gadolinium-enhanced T1-weighted MRI.

Gy in 30 fractions to the PTV, and additionally underwent simultaneous integrated boost targeting the hypercellular/hyperperfused tumor volume. A 0.5-cm margin was applied to the hypercellular/hyperperfused tumor volume to create a PTV_{boost} (no CTV margin was applied) and treated to 75 Gy in 30 fractions. The initial 10 dose-escalation trial patients underwent targeting of the TV_{HCV}, and the remaining patients to the combined TV_{HCV}/TV_{CBV} following analyses demonstrating the improving prognostic significance of the combination of imaging techniques.⁴ All patients were treated with concurrent (75 mg/m²) and adjuvant (150-200 mg/m² days 1-5 of a 28-day cycle) temozolomide for 6-12 cycles.

After progression, treatment was individualized and most commonly consisted of nitrosourea-based chemotherapy, with a minority of patients undergoing resection and/or re-irradiation.

Advanced Imaging Protocols

All imaging was acquired on a single 3T scanner (Skyra, Siemens Healthineers, Erlangen, Germany) using a 20-channel head coil in the Department of Radiation

Oncology at the University of Michigan. For the MRI acquisition protocols, conventional images including 2-dimensional (2D) T2-FLAIR, and 3-dimensional (3D) pre- and post-contrast T1-weighted images were obtained. DW-MR images were acquired using a 2D echo planar or RESOLVE pulse sequence with diffusion weighting in 3 orthogonal directions and b values of 0 and 3000 s/mm², as previously published.^{4,5} The RESOLVE diffusion pulse sequence reduces susceptibility artifacts that cause distortion, compared to conventional diffusion sequences. DCE images were acquired using a 3D gradient echo pulse sequence (TWIST) in the sagittal orientation to avoid arterial in-flow effect and ensure arterial coverage for input function delineation. Acquisition parameters for whole-brain coverage and T1 quantification have been previously defined.^{4,7} A three-parameter Tofts model was used to quantify the fractional plasma volume (V_p), transfer constant of contrast (K^{trans}), and the fractional volume of extravascular, extracellular space (v_e) with model assumptions as previously published.^{4,5,8} All image processing was performed using an in-house functional image analysis tool (*imFIAT*), validated and benchmarked at the highest level (level 5) by the NCI Quantitative Imaging Network.^{9,10}

Delineation of Hypercellular and Hyperperfused Tumor Volumes

The hypercellular tumor volume (TV_{HCV}) was delineated on DW images with $b = 3000$ s/mm². A fully automated threshold method was used to generate TV_{HCV} based on the mean intensity of contralateral normal brain + 2SD on a voxel-by-voxel basis.⁴ The hyperperfused tumor volume (TV_{CBV}) was defined based on the uptake of contralateral normal frontal gray matter + 1SD. Due to the inherent difference in cerebral blood volume (CBV) values of gray matter and white matter, the normal gray matter of the contralateral normal frontal lobe (with higher CBV than white matter) was segmented and used to define the TV_{CBV} tumor volume. This method identifies TV_{CBV} tumor volumes predictive of PFS and OS.⁴

Survival Analysis and Statistical Methods

The primary aim of this study was to determine whether targeting hypercellular/hyperperfused tumor regions with dose-intensified RT would induce greater mid-therapy tumor reduction compared to a non-trial comparison cohort, and whether this mid-therapy response was predictive of patient survival. OS was defined as the interval from the start of RT to death from any cause. For patients who were not reported to have died at the end of the study, the last clinical follow-up or last contact date, whichever occurred later, was used as the censoring date. Patients were generally followed every 8 weeks after chemoradiation with clinical exam and MRI. PFS was defined as the interval from the start of RT to progression or death, whichever occurred first, and patients were censored at the time of last imaging follow-up. Progression was determined by a multidisciplinary tumor board, and worsened enhancement within 3 months of chemoradiation was generally managed by repeat imaging to rule out pseudoprogression. Progression was defined as worsened enhancement outside of the radiation field, or within the radiation field if progression was confirmed pathologically or with serial confirmatory imaging and clinical evaluation, or by change in therapy (ie, initiation of next-line chemotherapy), whichever occurred first.

PFS and OS were calculated using the Kaplan-Meier method and subgroups were compared using the log-rank test. Wilcoxon signed-rank test was used to compare anatomic MRI-defined tumor volumes (based on T1-weighted gadolinium-enhanced and T2/FLAIR imaging), and advanced MRI-defined tumor volumes between dose-escalation trial and non-trial patients. Univariable Cox proportional hazards models were used to correlate PFS and OS with age, gender, Eastern Cooperative Oncology Group (ECOG) performance status (0 vs 1 vs 2), RT dose coverage of imaging volume ($\geq 95\%$ vs $< 95\%$, and continuous), extent of surgery (gross total resection vs subtotal resection vs biopsy alone), O⁶-methylguanine-DNA methyltransferase (MGMT) methylation (methylated, unmethylated, unknown), baseline anatomic (TV_{Gd} , TV_{FLAIR}) and advanced MRI (TV_{HCV} , TV_{CBV} , combined TV_{HCV}/TV_{CBV}) tumor volumes and their mid-radiation changes. Multivariable Cox proportional hazards models were generated to assess the

effect of anatomic and advanced MRI tumor volumes and their mid-radiation changes on PFS and OS, adjusting for age, MGMT methylation status, and extent of residual contrast-enhancing tumor.

Statistical analyses were performed using R (version 3.6.1). For all analyses, two-sided *P* values of $< .05$ were considered statistically significant, and values $< .1$ were considered a marginal association. Confidence intervals (CI) estimates were two-sided and set at 95%.

Results

Clinical Patient and Treatment Characteristics

Forty-nine patients with newly diagnosed GBM treated between October 2012 and December 2018 were included in this analysis. The median age was 58 years old (IQR 54-65). The majority (88%) of patients were of ECOG performance status 0-1 and underwent gross total resection (47%) or subtotal resection (37%). Only 6% of patients had IDH1 mutation. Patients enrolled on the Phase II dose-escalation trial were of older median age than the non-trial cohort (62 vs 55 years old, $P = .02$) and had a greater percentage of MGMT-unmethylated patients (73% vs 39%, $P = .002$), although 35% of patients treated in the non-trial cohort were lacking MGMT status due to the slightly earlier era of treatment before routine acquisition of this assay (Table 1).

Comparison of Anatomic and Advanced MRI Tumor Volumes

Among all patients, 35% (range 0%-91%) of the combined hypercellular/hyperperfused tumor volume was non-enhancing and extended outside of the conventional contrast-enhancing region (TV_{Gd}) prior to radiation therapy, which did not significantly differ between the dose-escalation trial and non-trial cohorts (35% for both). A significantly greater reduction in the combined hypercellular/hyperperfused (TV_{HCV}/TV_{CBV}) tumor volume was observed among patients treated in the dose-escalation trial cohort (3 cc reduction, IQR 2-5, or 41% reduction) vs the non-trial cohort (1 cc reduction, IQR 1-3, or 6% reduction, $P = .002$) (Figure 2, Panel A). However, even with dose-escalated radiotherapy at 2.5 Gy per fraction (75 Gy in 30 fractions), a subset of patients experienced less pronounced tumor reduction or even growth of the TV_{HCV}/TV_{CBV} tumor volume during treatment (Figure 2, Panel A). The hypercellular tumor component (TV_{HCV}), of specific utility in identifying non-enhancing tumor regions potentially missed by conventional MRI, was markedly reduced with dose-escalated radiation compared to standard treatment (71% reduction [IQR 34%-90%] vs 5% increase [IQR -23% to 17%], $P < .001$) (Table 2). The hyperperfused TV_{CBV} demonstrated greater heterogeneity of response, although overall reduction was observed among patients receiving dose-escalated RT (9% reduction, Table 2). Like the advanced MR-identified tumor volumes, the anatomic enhancing tumor volume TV_{Gd} (excluding surgical cavity) was also significantly reduced in the dose-escalation trial cohort compared to the non-trial cohort (40% reduction vs 16% reduction, Table 2).

Table 1 Patients Characteristics

	Dose-Escalation Trial Cohort	Non-Trial Cohort	PValue
Count			
N	26	23	
Age			
Median (IQR)	62 (56, 67)	55 (52, 59)	.02
Gender			
Female	10 (38.5)	7 (30.4)	
Male	16 (61.5)	16 (69.6)	.76
ECOG			
0	6 (23.1)	8 (34.8)	
1	18 (69.2)	11 (47.8)	
2	2 (7.7)	4 (17.4)	.35
Physical dose			
Median (IQR)	75 (75, 75)	60 (60, 72)	<.001
Extent of surgery			
Biopsy	3 (11.5)	4 (17.4)	
Subtotal resection	8 (30.8)	9 (39.1)	
Gross total resection	15 (57.7)	10 (43.5)	.67
MGMT methylation			
Positive	6 (23.1)	6 (26.1)	
Negative	19 (73.1)	9 (39.1)	
Unknown	1 (3.8)	8 (34.8)	.002
IDH status			
Mutant	1 (3.8)	2 (8.7)	
Wild-type	24 (92.3)	17 (73.9)	
Unknown	1 (3.8)	4 (17.4)	.22

Abbreviations: ECOG, Eastern Cooperative Oncology Group; IDH, isocitrate dehydrogenase; IQR, interquartile range; MGMT, 0⁶-methylguanine-DNA methyltransferase.

No difference in mid-RT anatomic tumor volumes (TV_{Gdr} , TV_{FLAIR} , $P > .3$ for both), and no difference in mid-RT advanced TV_{HCV}/TV_{CBV} tumor volumes ($P = .29$) was appreciated between MGMT-methylated vs -unmethylated patients.

Survival Outcomes Predicted by Hypercellular/Hyperperfused Tumor Response

The median follow-up time was 38 months (95% CI 27-50 months). Among all patients, median OS was 19 months (95% CI 16-28) and PFS was 11 months (95% CI 8-19). Trial patients treated with dose-escalated radiation targeting hypercellular/hyperperfused tumor regions had a median OS of 20 months (95% CI 18-not reached [NR]), and median PFS of 12 months (95% CI 10-17 months).¹¹ Patients with a larger reduction in the hypercellular/hyperperfused tumor volume during the radiation course had a substantially improved OS of 28 months (95% CI 18-NR) vs 16 months (95% CI 8-23 months) ($P = .04$) (Figure 2, Panel B).

Univariable analysis demonstrated that MGMT promoter methylation was associated with improved PFS (hazard ratio [HR] 0.33, 95% CI 0.13-0.83, $P = .02$). Increasing age (per year, HR 1.06, 95% CI 1.01-1.11, $P = .01$) and increase in the hyperperfused tumor volume (TV_{CBV}) during radiation (per 10% increase, HR 1.07, 95% CI 1.02-1.13, $P = .01$) were associated with worse OS. A trend to worse OS was observed with increasing TV_{HCV}/TV_{CBV} during radiation (per 10% increase, HR 1.12, 95% CI 0.99-1.27, $P = .08$).

In a multivariable analysis adjusting for known prognostic factors including age, MGMT methylation status, and the volume of postoperative residual enhancing tumor, an increase in the hypercellular/hyperperfused tumor volume (TV_{HCV}/TV_{CBV}) during radiation was associated with worse PFS (HR 1.16, 95% CI 1.01-1.32, $P = .03$) and worse OS (HR 1.21, 95% CI 1.04-1.41, $P = .02$) (Table 3) (Supplementary Figure 3). In contrast, the anatomic change in the mid-radiation volume of enhancement was not associated with survival ($P = .87$).

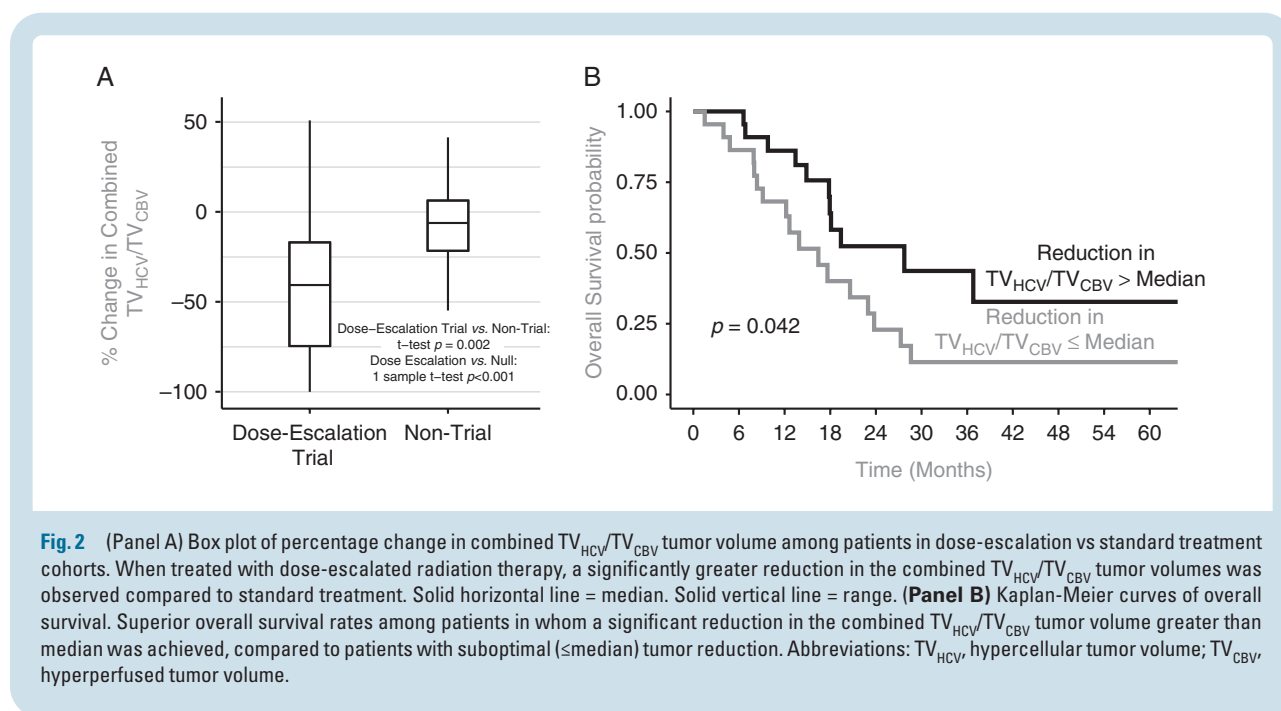
Correlation of Tumor Recurrence With Mid-Radiation TV_{HCV}/TV_{CBV}

All patients with measurable, mid-radiation TV_{HCV}/TV_{CBV} demonstrated spatial overlap of the mid-radiation TV_{HCV}/TV_{CBV} and eventual, enhancing tumor recurrence (Figure 3). In response to dose-escalated RT, one patient with an MGMT-methylated, IDH unknown tumor demonstrated complete response of the TV_{HCV}/TV_{CBV} by mid-radiation, with durable control of the index site but eventual tumor recurrence 2 years after treatment that was remote from the initial site.

Among the dose-escalation trial cohort, the mean persistent TV_{HCV}/TV_{CBV} (overlap of the pre-radiation and mid-radiation TV_{HCV}/TV_{CBV}) was 3.7 cc (IQR 0.8-5.1) and comprised approximately 40% of the total mid-radiation TV_{HCV}/TV_{CBV} . The remainder of the TV_{HCV}/TV_{CBV} that was developing during the course of radiation (extending outside of the initial TV_{HCV}/TV_{CBV}) was 4.7 cc (IQR 1.2-6.0). Approximately 30% (IQR 8%-64%) of the mid-radiation TV_{HCV}/TV_{CBV} extended outside of the 75 Gy boost dose region by mid-treatment, although no measurable TV_{HCV}/TV_{CBV} extended outside of the 95% (60 Gy) isodose line among patients undergoing dose-escalated targeting of the hypercellular/hyperperfused tumor from the start of treatment.

Toxicity of Dose-Escalation Trial Cohort

All patients were followed until last follow-up or death for late neurologic toxicity (median follow-up time 26 months (95% CI 19-NR)). Dose-escalated chemoradiation to 75 Gy was well tolerated in the trial cohort, with only 2 patients experiencing irreversible, late grade 3 neurologic toxicity.¹¹ The first patient had an MGMT-unmethylated tumor and experienced worsening seizures without corresponding radiographic changes 10 months' post-radiation, requiring titration of anti-seizure medications and initiation of bevacizumab. The second patient had an MGMT-methylated tumor, and experienced radiographic changes and biopsy-confirmed radiation necrosis with hemiparesis,



gait- and word-finding difficulty 17 months' post-radiation, requiring bevacizumab. No late grade 4-5 neurologic events occurred, suggesting further potential to improve the therapeutic ratio.

Discussion

In this study, we demonstrated that targeting an aggressive hypercellular/hyperperfused imaging phenotype⁴ with higher radiation dose yielded greater mid-therapy tumor reduction that was associated with superior survival in patients with GBM. Importantly, insufficient response of the hyperperfused/hypercellular tumor volume by mid-radiation was associated with significantly worse PFS and OS, independent of age, extent of residual enhancing disease, and MGMT methylation. These findings support the potential importance of intensifying radiation dose against these tumor regions from the start of treatment, and provide an avenue to further improve the therapeutic index by identifying persistent and developing regions of treatment resistance *during radiation* that would benefit from further, selective dose-intensification for the remainder of therapy.

Typically, anatomic MR imaging is acquired after resection for radiation treatment planning and is not repeated until 1 month after completion of radiation. For centers that employ a sequential boost, an interim MRI may be repeated during the course of chemoradiation for boost planning. Because increases in enhancement that occur during treatment may be due to the nonspecific effects of radiation and chemotherapy,¹² and in limited studies have not demonstrated significant association with PFS or OS in brain tumor patients, interim conventional MRI during chemoradiation is not standardly acquired for tumor assessment or early prognostication. In our study,

no association was demonstrated between quantitative changes in anatomic enhancing tumor volume and patient outcome.

Relatively few studies have evaluated advanced imaging changes during chemoradiation in patients with GBM, and their association with patient outcome. These studies have demonstrated detectable and quantifiable tumor and microenvironmental changes 3-4 weeks into radiation using advanced MRI techniques compared to pre-treatment that correlate with early progression and even OS. In a study of 18 patients¹³ with newly diagnosed GBM undergoing pre-RT and third week 3D-MR proton spectroscopic imaging, a voxel-by-voxel analysis assessing for abnormal activity (choline/N-acetyl aspartate ratio, or Cho/NAA) ≥ 2 demonstrated that decreased or stable mean or median Cho/NAA values had lower risk of progression. In contrast, an increase in mean or median Cho/NAA values by week 3 of RT had significantly greater chance of early progression (both $P < .01$, HR 2.72 (95% CI 1.10-6.71, $P = .03$). Despite receiving standard ~ 60 Gy radiation dose to this metabolic abnormality, most recurrences occurred in this region, and dose-escalation against these tumor regions is the subject of an ongoing study.^{13,14} Other studies have utilized functional imaging techniques to assess whether changes in tumor vasculature and perfusion characteristics during radiation are associated with OS. In a study of 22 patients with GBM,¹⁵ a greater mid-RT reduction in K^{trans} values was observed among responders vs non-responders ($P = .04$), possibly due to early reduction in vascular leakiness leading to enhanced oxygenation and therapeutic efficacy. Subsequent studies have more specifically evaluated regional changes in elevated CBV within heterogeneous glioma subregions as a metric of tumor response during treatment. In a prior series of 23 patients¹⁶ with newly diagnosed high-grade gliomas, we found that a decrease in the fractional high CBV tumor regions during week 3 vs week

Table 2 Comparison of Conventional and Advanced Imaging Volumes by Treatment Type (in Cubic Centimeters)

	Dose-Escalation Trial: Baseline	Non-Trial: Baseline	P Value	Dose-Escalation Trial: Mid-RT	Non-Trial: Mid-RT	P Value	Dose-Escalation Trial: Absolute Change	Non-Trial: Absolute Change	P Value	Dose-Escalation Trial: % Change	Non-Trial: % Change	P Value
Count												
N	26	23		26	23		26	23		26	23	
Enhancing tumor (TV _{Gd})												
Median (IQR)	16.8 (10.1, 30.6)	24.2 (17.5, 39.8)	.08	9.9 (5.2, 18.6)	26.0 (15.7, 37.3)	<.01	-5.8 (-10.5, -2.4)	-1.6 (-6.0, 3.9)	.13	-39.9 (-56.2, -25.1)	-16.0 (-25.9, 17.0)	.01
FLAIR volume (TV _{FLAIR})												
Median (IQR)	71.4 (40.3, 118.2)	67.8 (43.4, 96.7)	0.01	43.9 (26.6, 79.3)	58.2 (40.8, 95.3)	.34	-22.7 (-52.1, -3.1)	-3.2 (-13.5, 2.3)	.41	-33.3 (-47.3, -22.7)	-3.7 (-24.7, 3.7)	.02
Hypercellular tumor (TV _{HCV})												
Median (IQR)	5.9 (3.2, 10.8)	7.6 (4.4, 11.4)	<.01	1.7 (0.7, 3.6)	7.9 (1.7, 12.0)	.04	-3.6 (-5.9, -1.6)	0.3 (-3.3, 2.7)	.19	-70.8 (-90.4, -33.9)	4.9 (-30.2, 23.1)	<.01
Hyperperfused tumor (TV _{CBV})												
Median (IQR)	4.3 (1.8, 9.3)	5.7 (2.2, 17.2)	.53	4.1 (1.1, 8.9)	7.7 (0.9, 19.1)	.05	-0.4 (-1.1, 1.0)	-0.1 (-1.8, 0.7)	.17	-8.9 (-70.6, 18.5)	-2.5 (-23.2, 17.0)	.60
Combined TV _{HCV} /TV _{CBV}												
Median (IQR)	9.0 (6.1, 18.6)	12.6 (8.0, 26.1)	.02	5.7 (2.3, 13.4)	12.0 (6.1, 28.7)	.03	-2.9 (-5.3, -1.8)	-0.5 (-3.1, 1.3)	.15	-40.6 (-74.5, -16.9)	-6.1 (-21.6, 6.4)	<.01

Abbreviations: FLAIR, fluid-attenuated inversion recovery; IQR, interquartile range; RT, radiation therapy.

Table 3 Cox Proportional Hazards Models for Progression-Free Survival and Overall Survival

	HR (95% CI)	PValue
Progression-free survival		
MGMT-methylated (positive vs negative)	0.25 (0.08-0.76)	.015
Baseline TV _{Gd} volume (per 10 cc)	0.86 (0.67-1.11)	.250
Mid-radiation change in combined TV _{HCV} /TV _{CBV} volume (per 10%)	1.16 (1.01-1.32)	.032
Overall survival		
Age (per 5 years)	1.43 (1.04-1.96)	.027
MGMT-methylated (positive vs negative)	0.44 (0.17-1.16)	.098
Mid-radiation change in combined TV _{HCV} /TV _{CBV} volume (per 10%)	1.21 (1.04-1.41)	.015

Abbreviations: CI, confidence intervals; HR, hazard ratio; MGMT, O⁶-methylguanine-DNA methyltransferase; TV_{CBV}, hyperperfused tumor volume; TV_{Gd}, gadolinium-enhancing tumor volume; TV_{HCV}, hypercellular tumor volume. Significant *P* values are depicted in bold text.

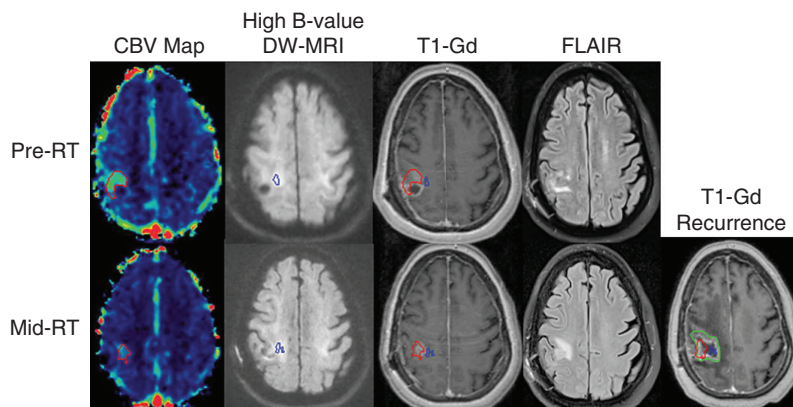


Fig. 3 Correlation between persistent and developing mid-radiation hyperperfused and hypercellular tumor volumes and tumor recurrence. A hyperperfused region of tumor (red volume, far left column) extending outside of the enhancing target (third column, upper panel) demonstrates resolution laterally but persistence medially by mid-RT. A geographically distinct but also non-enhancing hypercellular region of tumor (blue volume, second column) demonstrates persistent but also newly developing regions of tumor further medially by mid-RT, while the enhancing target regresses (third column, bottom panel). Both persistent and developing hyperperfused and hypercellular tumor volumes detected mid-radiation correspond to the eventual tumor recurrence (green volume, far right panel) 8 months after chemoradiation. Abbreviations: CBV, cerebral blood volume; DW-MRI, diffusion-weighted magnetic resonance image; FLAIR, fluid-attenuated inversion recovery; RT, radiation; T1-Gd, gadolinium-enhanced T1-weighted MRI.

1 of radiation was independently associated with better survival, and could potentially serve as a metric of early tumor response or therapeutic resistance. Another study of 45 high-grade glioma patients¹⁷ incorporating perfusion as well as diffusion MRI demonstrated that regional decreases in rCBV and increases in apparent diffusion coefficient (ADC) assessed by parametric response method in the first 3 weeks of treatment correlated with survival. Similar to our prior findings,³ additional series¹⁸ suggest that the predictive value of diffusion MRI in assessing early changes correlated with later tumor response is enhanced with high *b* value DW-MRI ($b = 3000\text{-}4000$ s/mm²) compared to conventional ADC maps.

Advanced positron emission tomography (PET) tracers have similarly been used to noninvasively interrogate the

heterogeneous biology of malignant gliomas,¹ although comparative studies assessing advanced PET imaging vs advanced MRI techniques in identifying biologically relevant tumor or predicting outcome are lacking. Studies of post-chemoradiation response of metabolic tumor volumes identified 2-3 months after treatment using ¹¹C-methionine PET^{19,20} and *O*-(2-¹⁸F-fluoroethyl)-L-tyrosine (¹⁸F-FET) PET²¹ demonstrate improved PFS in newly diagnosed and recurrent GBM. However, whether evolving response or treatment resistance may be identified earlier, even during the course of radiation, using advanced PET techniques has not been evaluated.

In our study, we assessed the significance of mid-therapy changes in an advanced MR biomarker identifying an adversely prognostic^{3,4} hypercellular and hyperperfused

imaging phenotype that is unique in that it may be feasibly and justifiably targeted⁵ with precision, dose-escalated radiotherapy. GBM tumor evolution is a spatially and temporally dynamic process potentially accelerated by temozolomide and radiation. Preclinical and clinical evidence support that radiation therapy and temozolomide contribute to evolving mutation patterns, the presence and clonality of driver mutations, and subpopulation evolution.^{22,23} Sequencing of matched primary-recurrent GBM samples from patients receiving standard chemoradiation therapy demonstrate GBM driver instability,²² and underscore the importance of identifying a noninvasive method of assessing spatiotemporal tumor evolution. Our findings correlating suboptimal response of hypercellular and hyperperfused tumor regions with worse survival suggest that this technique may identify treatment-resistant tumor regions early during treatment. These tumor regions were often spatially disparate, and the hypercellular tumor regions were often not hyperperfused. Whether these hypercellular tumor regions contain more hypoxic and potentially radioresistant tumor niches will require further study. A next logical step is determining whether persistent or developing regions of treatment resistance identified mid-radiation using this imaging technique may be targeted with adaptive re-planning, selectively intensifying dose against these tumor regions to improve outcomes with acceptable safety. In our prior work, we have demonstrated that this advanced imaging signature may be feasibly integrated into the clinical workflow for patient care,⁵ and implemented for tumor targeting using precision radiotherapy techniques in a recently completed phase II trial that demonstrated early promising outcomes when the hypercellular/hyperperfused tumor regions are identified prior to radiation and targeted with dose-escalated radiation therapy.¹¹ In the present analysis, we demonstrated particularly favorable outcomes among the subset of identifiable patients with an early response of this imaging signature after radiation therapy commenced, but during the radiation course. Additionally, the mid-therapy hypercellular/hyperperfused tumor volumes demonstrated spatial concordance with regions of eventual tumor recurrence, suggesting its potential to identify relevant regions of evolving treatment resistance during radiation therapy. Approximately 30% of the mid-therapy hypercellular/hyperperfused tumor volume developing during the course of treatment extended outside of the 75 Gy boost region by mid-therapy, and would be potentially targetable with an adaptive re-planning strategy. Ongoing and future directions include patient-specific adaptation with dose-intensified RT using this imaging biomarker to identify treatment resistance during radiation that would benefit from even higher, but more targeted dose, and characterization of the molecular signatures corresponding to the hypercellular and hyperperfused imaging phenotypes to inform adjuvant treatment strategies and select patients who may benefit from this treatment approach.

Limitations of this study include the non-randomized comparison and sample size. Validation of the significance of the persistent and developing tumor regions

identified with this multiparametric MR imaging technique will require definitive assessment in the setting of a multicenter randomized trial. Additionally, while radiation dose-escalation using conventional imaging techniques has yet to demonstrate survival benefit, with recent negative outcomes in the photon cohort of the ongoing NRG BN001 trial, the potential benefit of implementing biologically informed imaging techniques to adequately target even non-enhancing tumor regions with intensified local therapy potentially adapted during the radiation course remains an unanswered question to be addressed in future studies.

In conclusion, we demonstrate the importance of a dose-intensification strategy against adversely prognostic hypercellular and hyperperfused tumor regions, whose persistence and development during radiation is independently associated with survival, correlated with eventual tumor recurrence, and may potentially be targeted with adaptive, individualized radiation therapy using an advanced imaging strategy to detect therapeutic resistance. Given the variability of response that we observed, early patient characterization using both molecular and advanced imaging techniques is needed to identify patients in whom a dose-intensification strategy is likely to achieve long-term tumor control and to significantly enhance survival.

Supplementary Material

Supplementary material is available at *Neuro-Oncology* online.

Keywords

glioblastoma | multiparametric MRI | overall survival | radiation therapy | response assessment

Funding

This study was supported in part by NIH P01 CA059827 and Cancer Center Support Grant P30 CA046592.

Conflict of interest statement. None.

Authorship statement. Experimental design: M.M.K., Y.S., T.S.L., Y.C. Implementation: M.M.K., M.P.A., H.A.P., D.R.W., T.S.L., Y.C. Analysis: M.M.K., M.P.A., Y.S., H.A.P., P.L., M.S., D.R.W., T.S.L., Y.C. Interpretation of data: M.M.K., M.P.A., Y.S., H.A.P., P.L., M.S., D.R.W., T.S.L., Y.C.

References

1. Albert NL, Weller M, Suchorska B, et al. Response Assessment in Neuro-Oncology working group and European Association for Neuro-Oncology recommendations for the clinical use of PET imaging in gliomas. *Neuro Oncol*. 2016;18(9):1199–1208.
2. Hygino da Cruz LC Jr, Rodriguez I, Domingues RC, Gasparetto EL, Sorensen AG. Pseudoprogression and pseudoresponse: imaging challenges in the assessment of posttreatment glioma. *AJNR Am J Neuroradiol*. 2011;32(11):1978–1985.
3. Pramanik PP, Parmar HA, Mammoser AG, et al. Hypercellularity components of glioblastoma identified by high b-value diffusion-weighted imaging. *Int J Radiat Oncol Biol Phys*. 2015;92(4):811–819.
4. Wahl DR, Kim MM, Aryal MP, et al. Combining perfusion and high b-value diffusion MRI to inform prognosis and predict failure patterns in glioblastoma. *Int J Radiat Oncol Biol Phys*. 2018;102(4):757–764.
5. Kim MM, Parmar HA, Aryal MP, et al. Developing a pipeline for multiparametric MRI-guided radiation therapy: initial results from a phase II clinical trial in newly diagnosed glioblastoma. *Tomography*. 2019;5(1):118–126.
6. Stupp R, Mason WP, van den Bent MJ, et al.; European Organisation for Research and Treatment of Cancer Brain Tumor and Radiotherapy Groups; National Cancer Institute of Canada Clinical Trials Group. Radiotherapy plus concomitant and adjuvant temozolomide for glioblastoma. *N Engl J Med*. 2005;352(10):987–996.
7. Bane O, Hectors SJ, Wagner M, et al. Accuracy, repeatability, and interplatform reproducibility of T1 quantification methods used for DCE-MRI: results from a multicenter phantom study. *Magn Reson Med*. 2018;79(5):2564–2575.
8. Cao Y, Li D, Shen Z, Normolle D. Sensitivity of quantitative metrics derived from DCE MRI and a pharmacokinetic model to image quality and acquisition parameters. *Acad Radiol*. 2010;17(4):468–478.
9. Cao Y, Shen Z. SU-FF-J-117: integrated software tools for multimodality functional images in cancer clinical trials. *Med Phys*. 2007;34:2395.
10. Farahani K, Kalpathy-Cramer J, Chenevert TL, et al. Computational challenges and collaborative projects in the NCI quantitative imaging network. *Tomography*. 2016;2(4):242–249.
11. Kim MM, Sun Y, Aryal MP, et al. A phase 2 study of dose-intensified chemoradiation using biologically based target volume definition in patients with newly diagnosed glioblastoma. *Int J Radiat Oncol Biol Phys*. 2021. doi:10.1016/j.ijrobp.2021.01.033.
12. Cao Y, Tsien CI, Shen Z, et al. Use of magnetic resonance imaging to assess blood-brain/blood-glioma barrier opening during conformal radiotherapy. *J Clin Oncol*. 2005;23(18):4127–4136.
13. Muruganandham M, Clerkin PP, Smith BJ, et al. 3-Dimensional magnetic resonance spectroscopic imaging at 3 Tesla for early response assessment of glioblastoma patients during external beam radiation therapy. *Int J Radiat Oncol Biol Phys*. 2014;90(1):181–189.
14. Laprie A, Ken S, Filleron T, et al. Dose-painting multicenter phase III trial in newly diagnosed glioblastoma: the SPECTRO-GLIO trial comparing arm A standard radiochemotherapy to arm B radiochemotherapy with simultaneous integrated boost guided by MR spectroscopic imaging. *BMC Cancer*. 2019;19(1):167.
15. Bisdas S, Smrdel U, Bajrovic FF, Surlan-Popovic K. Assessment of progression-free-survival in glioblastomas by intratreatment dynamic contrast-enhanced MRI. *Clin Neuroradiol*. 2016;26(1):39–45.
16. Cao Y, Tsien CI, Nagesh V, et al. Survival prediction in high-grade gliomas by MRI perfusion before and during early stage of RT [corrected]. *Int J Radiat Oncol Biol Phys*. 2006;64(3):876–885.
17. Galbán CJ, Chenevert TL, Meyer CR, et al. Prospective analysis of parametric response map-derived MRI biomarkers: identification of early and distinct glioma response patterns not predicted by standard radiographic assessment. *Clin Cancer Res*. 2011;17(14):4751–4760.
18. Mardor Y, Pfeffer R, Spiegelmann R, et al. Early detection of response to radiation therapy in patients with brain malignancies using conventional and high b-value diffusion-weighted magnetic resonance imaging. *J Clin Oncol*. 2003;21(6):1094–1100.
19. Miller S, Li P, Schipper M, et al. Metabolic tumor volume response assessment using ¹¹C-methionine positron emission tomography identifies glioblastoma tumor subregions that predict progression better than baseline or anatomic magnetic resonance imaging alone. *Adv Radiat Oncol*. 2020;5(1):53–61.
20. Galldiks N, Kracht LW, Burghaus L, et al. Use of ¹¹C-methionine PET to monitor the effects of temozolomide chemotherapy in malignant gliomas. *Eur J Nucl Med Mol Imaging*. 2006;33(5):516–524.
21. Galldiks N, Langen KJ, Holy R, et al. Assessment of treatment response in patients with glioblastoma using O-(2-¹⁸F-fluoroethyl)-L-tyrosine PET in comparison to MRI. *J Nucl Med*. 2012;53(7):1048–1057.
22. Draaisma K, Chatzili A, Taphoorn M, et al. Molecular evolution of IDH wild-type glioblastomas treated with standard of care affects survival and design of precision medicine trials: a report from the EORTC 1542 study. *J Clin Oncol*. 2020;38(1):81–99.
23. McAbee JH, Rath BH, Valdez K, et al. Radiation drives the evolution of orthotopic xenografts initiated from glioblastoma stem-like cells. *Cancer Res*. 2019;79(23):6032–6043.